Applied Catalysis B: Environmental 242 (2019) 284–292

Contents lists available at ScienceDirect

Applied Catalysis B: Environmental

journal homepage: www.elsevier.com/locate/apcatb

Photocatalytic degradation of organic pollutant with polypyrrole nanostructures under UV and visible light

Xiaojiao Yuan[a], Dita Floresyona[a], Pierre-Henri Aubert[b], Thanh-Tuân Bui[b], Samy Remita[a,c], Srabanti Ghosh[a,1], François Brisset[d], Fabrice Goubard[b], Hynd Remita[a,e,*]

[a] Laboratoire de Chimie Physique, UMR 8000 CNRS, Université Paris-Sud, Université Paris-Saclay, 91405 Orsay, France
[b] Laboratoire de Physicochimie des Polymères et des Interfaces (LPPI, EA 2528), Université de Cergy-Pontoise, F-95031 Neuville-sur-Oise Cedex, France
[c] Département Chimie Vivant Santé, EPN 7, Conservatoire National des Arts et Métiers, CNAM, 292 rue Saint-Martin, 75141 Paris Cedex 03, France
[d] Institut de Chimie Moléculaire et des Matériaux d'Orsay, ICMMO, UMR 8182 CNRS, Université Paris-Sud, Université Paris Saclay, Bât 410-420, Orsay F-91405, France
[e] CNRS, Laboratoire de Chimie Physique, UMR 8000, 91405 Orsay, France

ARTICLE INFO

Keywords:
Polypyrrole
Conjugated polymers
Nanostructures
Photocatalysis
Water depollution

ABSTRACT

Conjugated polymer nanostructures (CPNs) emerge as a new class of photocatalysts for organic pollutant degradation under UV and visible light. Polyprrole (PPy), as a conjugated polymer, exhibits a wide range of applications. We present here the first demonstration of employing pure PPy nanostructures as a very efficient photocatalyst for water depollution. PPy nanostructures were synthesized in hexagonal mesophases (used as soft templates) by chemical polymerization (PPy-NS-c), obtained by radiolysis (PPy-NS-γ), and synthesized without any template via chemical method (PPy-bulk) as bulk. The different PPy samples were characterized by SEM, TEM, FTIR and UV–vis absorption spectroscopy. The photocatalytic activity of both PPy nanostructures (PPy-NS-c and PPy-NS- γ), which remain very stable after several cycles, was evaluated for the degradation of organic pollutant in aqueous solution (phenol and methyl orange were taken as a model pollutant). PPy nanostructures show high photocatalytic activity under both UV and visible light while bulk PPy (PPy-bulk) has no appreciable activity. PPy-NS-c present the highest activity for photodegradation of phenol under UV light, while PPy-NS-γ exhibit the best photocatalytic activity under visible light. We demonstrate here that the nanostructuration of these polymers is an important factor for their application in photocatalysis.

1. Introduction

Titanium dioxide is the most widely used photocatalyst because of its nontoxicity, mechanical stability, corrosion resistance, high photocatalytic activity and low price [1]. Nevertheless, TiO_2 is only active under UV light because of its large band gap (3.2 eV for anatase and 3.0 eV for rutile), which constitutes 3–4 % of the solar light impinging on the Earth's surface. To overcome this limitation and extend its photocatalytic activity toward the visible region, a huge number of efforts have been made either via doping of TiO_2 with N, C or S or by its surface modification with metal nanoparticles (NPs) such as Ag, Au, Pt, Pd NPs [2–10].

Besides, the development of efficient, durable and cost-effective materials for photocatalytic applications and solar energy conversion is crucial for environmental applications and solar fuel production. In this context, different semiconductor nanostructures and novel photocatalysts have been proposed for solar energy conversion such as bismuth-based oxides [11,12], lanthanide stannates [13–16], spinel compounds [17], ZnO-based nanocomposites [18], graphene oxides [19–21] and conducting polymer nanostructures [22,23].

Since MacDiarmid and co-workers discovered conducting polyacetylene (PA) doped with iodine in 1977, conducting polymers (CPs) have drawn much attention for energy conversion and storage applications such as solar cells, fuel cells and rechargeable lithium batteries [24–31]. Conducting polymers offer the advantages of their low cost, facile synthesis, excellent electrochemical performance, great electrical conductivity and high carrier mobility. Conjugated polymers as a new class of photocatalysts, is very active under UV and visible light [22,23,32,33]. Novel organic polymeric based materials have recently made an upsurge in photocatalysis and solar energy conversion [34]. For example, g-C_3N_4 is a thermally and chemically stable semiconducting material that was discovered to photocatalyze a wide

* Corresponding author at: Laboratoire de Chimie Physique, UMR 8000 CNRS, Université Paris-Sud, Université Paris-Saclay, 91405 Orsay, France.
E-mail address: hynd.remita@u-psud.fr (H. Remita).
[1] Present address: Fuel Cell & Battery division, CSIR-Central Glass and Ceramic Research Institute, 196, Raja S.C. Mullick Road, Kolkata- 700032, India

https://doi.org/10.1016/j.apcatb.2018.10.002
Received 20 July 2018; Received in revised form 28 September 2018; Accepted 2 October 2018
Available online 05 October 2018
0926-3373/

variety of chemical reactions including the water splitting reaction [35–39].

Recently, we developed an alternative radiolytic methodology to synthesize conducting polymer nanostructures (CPNs) either in aqueous solutions or in organic solvents thanks to the use of high-energy radiations [40–47]. Also, the controlled synthesis in soft templates (made of hexagonal mesophases) of conjugated polymer nanostructures such as poly(diphenylbutadyine) (PDPB) [48], poly(3,4-ethylenedioxythiophene) (PEDOT) [49], and poly(3-hexylthiophene) (P3HT) [23] has been reported by our group. We have demonstrated for the first time in the literature that these CPNs are highly active photocatalysts under UV and visible light, and more interestingly that their photocatalytic activity under visible irradiation is higher than that of plasmonic TiO_2 (titania modified with silver nanoparticles) [22]. In all cases, the polymer nanostructures were synthesized in soft templates made by hexagonal mesophases. In spite of using various methodology (radiolysis or photochemical polymerization for PDPB or chemical oxidation for PEDOT and P3HT), polymerization has always been shown to proceed in the confined hydrophobic domain (oil cylinders) of the hexagonal mesophases [50]. The as-prepared nanometric sized polymeric material can be extracted from the hexagonal mesophases by simple addition of ethanol [32,48,51,52]. Importantly, the beneficial role of the nanostructuration of the polymer for its photocatalytic activity in the visible region was clearly observed, since the bulk counterpart exhibited very low photocatalytic activity [23,49,50].

Polypyrrole (PPy) is considered as one of the well explored conjugated polymer for different applications such as actuators [53], supercapacitor electrodes [54,55], ablation of cancer cells [56,57], fuel cells, and catalysis [58] owing to its high electrical conductivity, high stability, high carrier mobility, excellent electrochemical activity, facile synthesis and strong binding or tethering sites for sequential reactions. A variety of synthesis methods such as templated-based and template-free synthesis have been developed to prepare PPy nanostructures of different morphologies [40]. Using soft templates, different morphologies were obtained by controlling the concentrations of the surfactants and that of the monomers [59,60]. For photocatalytic application in water treatment, composite nanomaterials based on PPy associated to inorganic semiconductors have been also developed such as polypyrrole-TiO_2 [61], AgCl/PPy [62], and PPy/$Bi_2O_2CO_3$ [63] etc.

Here, we demonstrate for the first-time the high photocatalytic activity of bare polypyrrole nanostructures for water treatment. We show that PPy conjugated polymers are highly efficient for degradation of organic pollutants (phenol taken as a model pollutant) under both ultraviolet and visible light irradiation. We report on the synthesis of PPy nanostructures with three different approaches: *i)* in soft templates using swollen hexagonal mesophases by chemical oxidation (PPy-NS-c), *ii)* in the absence of any template by direct gamma irradiation synthesis (PPy-NS-γ), and *iii)* without any templates by chemical oxidation (PPy-bulk). PPy nanostructures are stable under photocatalytic cycling. The photocatalytic activities of these PPy structures were investigated and compared. The photocatalytic mechanism was also studied and discussed in details.

2. Experimental section

2.1. Materials and reagents

Pyrrole (Py) (98%, Aldrich Chemical Co.), as monomer, iron (III) chloride ($FeCl_3$) as oxidative agent, sodium dodecyl sulfate (SDS) as surfactant, sodium chloride (NaCl), copper (II) sulfate pentahydrate (~99%), methyl orange (MO), cyclohexane (99.7%), phenol, 2-propanol (99.5%), tert-butanol (≥99.5%), ethanol (≥99% for HPLC) were purchased from Sigma-Aldrich, and n-pentanol was purchased from Honeywell (≥99%). All the reagents were analytically pure, commercially available and used without further purification. Ultrapure water (Millipore System, 18.2 MΩ cm) was used.

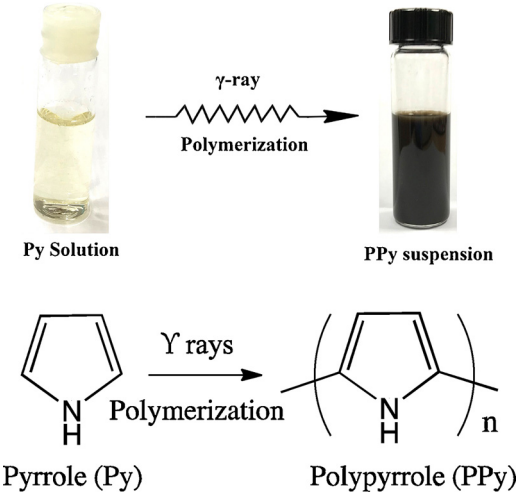

Scheme 1. PPy Polymerization by radiolysis.

2.2. Photocatalysts preparation

In this work, we used three methods to synthesize PPy:

(i) The as-prepared sample PPy-NS-γ was synthesized by radiolysis without any template and the color of the solution varied from the transparent solution (before irradiation) to black solution (after irradiation) (Scheme 1). PPy-NS-γ are obtained by oxidation of the Py monomer by $HO^{\bullet}$ radicals in water solution. The synthesis procedure was adapted from the ref. [40] with few modifications. In brief, an aqueous solution containing 20 mM pyrrole was degassed with N_2O for 20 min and irradiated with a ^{60}Co panoramic γ-source at a dose rate of 4.1 kG h^{-1}. The used dose was 77 kGy. After drying in the oven at 50 °C, a black powder was obtained: PPy-NS-γ.

(ii) PPy-NS-c nanostructures were synthesized by chemical oxidation of the PPy monomer confined in the oil phase of hexagonal mesophases (0.1 mM). Hexagonal mesophases are made of a mixture of sodium dodecyl sulfate (SDS) as surfactant, salted water phase (NaCl, and containing $FeCl_3$ and Py in this study), cyclohexane as oil phase and pentanol as cosurfactant. These mesophases are composed of oil-swollen surfactant tubes arranged on a triangular lattice in water and doped with Py monomer in water phases (in our case) were used as soft templates for the synthesis of PPy nanostructures. Formation of hexagonal mesophases was described in details in previous works [32,48,50–52]. As shown in Fig. 1, 7 µL Py was added to 2 mL of an aqueous solution containing 0.1 M NaCl, and 0.8 g SDS were introduced to the obtained solution. The mixture is vortexed for few minutes and then put in an oven at 50 °C for 1 h: A transparent viscous micellar solution (solution A) is obtained. 0.1 M $FeCl_3$ was dissolved in 2 mL of water. 0.8 g SDS is introduced in the solution and the mixture is mixed, vortexed and put in an oven at 50 °C for 1 h (solution B). Subsequently, 3 mL of cyclohexane was added to each micellar solution (solution A and B, respectively). The ratio monomer/oxidant [Py]/[$FeCl_3$] was 1/2. After vortexed a few minutes, 400 µL n-pentanol (co-surfactant) were added dropwise. The mixtures were then vortexed until a transparent (A) and yellow translucent (B), birefringent gels (hexagonal mesophases) were obtained. Mixing A and B lead to a black gel (C). During the process, the color of the mesophases changed very fast from transparent to black (Fig. 2). The PPy nanostructures were extracted by addition of ethanol, which destabilizes the mesophase. After centrifugation of the suspensions, PPy nanostructures were washed several times with ethanol and dried in the oven at 60 °C: A black powder (D) was then obtained.

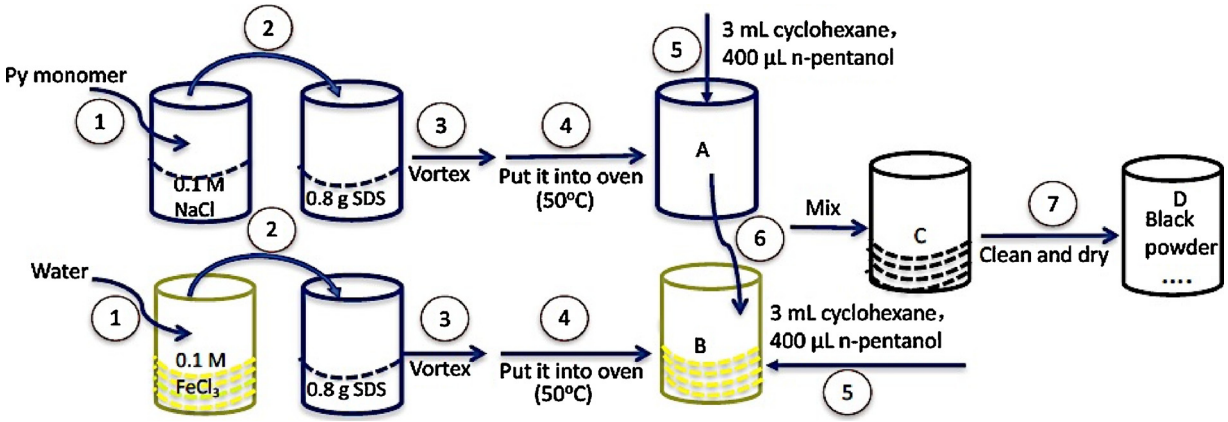

Fig. 1. The flow-process diagram of PPy-NS-c synthesis.

(iii) PPy-bulk was synthesized by chemical oxidation (using $FeCl_3$ as oxidant) in water without any surfactant nor irradiation. The ratio monomer/oxidant [Py]/ [$FeCl_3$] = 1/2 (the same ratio as that used for synthesis of PPy-NS-c). After centrifugation of the suspensions, bulk-PPy PPy were washed several times with ethanol and dried in the oven at 60 °C.

2.3. Characterization

The different materials were characterized by FT-IR, SEM, TEM, UV–vis absorption spectroscopy and Maldi-TOF.

Fourier transform infrared (FT-IR) spectra were obtained by using an FTIR spectrometer (Bruker Vertex 70) with a diamond ATR attachment (PIKEMIRACLE crystal plate diamond/ZnSe) and a MCT detector with a liquid nitrogen cooling system.

The morphologies and nanostructures of the solid samples were characterized by scanning electron microscopy (SEM, ZEISS Supra 55 V P FEG-SEM at 1 kV) and by transmission electron microscopy (TEM, JEOL JEM 100CX).

UV-Vis absorption spectra of PPy suspension were recorded with a UV–vis scanning spectrophotometer (HP 8453) in quartz cell.

Maldi-TOF (Matrix Assisted Laser Desorption/Ionization Time of Flight) mass spectrometry (Xevo Q-Tof WATERS) was used to determine the polymerization degree. The suspension of PPy in water was mixed with a matrix solution. The matrix solution was then placed on a stainless-steel plate. The spectra were obtained in the reflection mode and in the positive ion mode.

2.4. Electrical conductivity

To measure the electrical conductivity of PPy, the Kelvin four-point probe technique was used to measure the resistance of the as-prepared samples. Before measurements, PPy films were obtained by spin coating with a small drop of PPy suspensions on a glass substrate. The suspensions were doped with $NOBF_4$ (200 mM) in acetonitrile. A 3 Veeco Dektak 150 surface profiler was used to measure the thickness of the film.

According to the following equation, the conductivity (ρ, S cm^{-1}) was obtained:

$$\rho = \left(\frac{\pi}{\ln 2} \times \frac{V}{I} \times t\right)^{-1} \quad (1)$$

where V is the voltage (V), I is the applied current (A) and t is the thickness of the films (cm).

2.5. Electrochemical measurements

Cyclic voltammograms (CV) of PPy were measured by IUPAC. The oxidation potential (E_{ox}) of the CPs were measured in dichloromethane by cyclic voltammetry with tetrabutylammonium perchlorate (0.1 M) as a supporting electrolyte in a standard one-compartment, three-electrode electrochemical cell under argon: A VSP BioLogic potentiostat was used at a scan rate of 20 mV s^{-1}. Platinum disk (Ø = 1 mm), Ag wire pseudo-reference, and gold electrodes were used as working, reference and counter electrodes, respectively. Ferrocene was used as an internal standard, and the potentials were referred to the reversible formal potential of the compound.

2.6. Photocatalytic tests

The photocatalytic activity of PPy samples was evaluated for degradation of two model pollutants: phenol (C_6H_5OH, 50 ppm) and methyl orange (MO, 500 ppm). Before photocatalytic experiments, the suspensions containing the PPy and the model pollutant were stirred in the dark for 2 h to ensure adsorption-desorption equilibrium. Then, the suspension was exposed to light under stirring and O_2 bubbling. An Oriel 300 W Xenon lamp with an infrared water filter and a 400-nm cut off filter for the experiment under visible light was used as the light source. In details, 3 mg of PPy powder were added into 3 mL phenol aqueous solution with stirring. 300 µL of the suspension were taken out

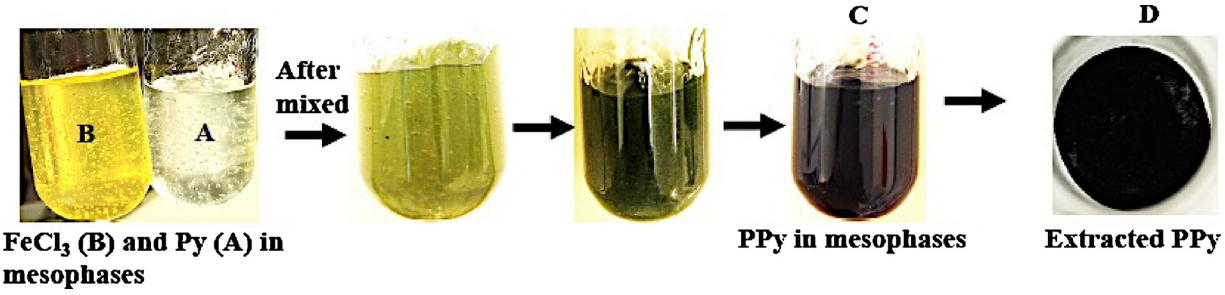

Fig. 2. Colour variation during the synthesis process in mesophases leading to PPy-NS-c.

every 1 h of irradiation and the mixture was centrifuged to remove the PPy nanostructures. High pressure liquid chromatography (HPLC) was used to determine the concentration of phenol and to calculate its photocatalytic degradation activity. Degradation of MO was followed by UV–vis spectrophotometric method at 460 nm wavelength. The degradation rate of phenol is expressed as $(C_0\text{-}C)/C_0 \times 100\%)$, where C_0 is the initial concentration of phenol and C represents the concentration of phenol after every interval of 1 h.

The mineralization of phenol was studied by the total organic carbon (TOC) using a Shimadzu TOC-LCSH.

Tris(hydroxymethyl) aminomethane (noted Tris) was used as a probe to determine the hydroxyl radical concentration [22,49,64]. Hydroxyl radicals and formaldehyde are produced during the reaction between Tris and hydrogen-abstracting species. The quantification of the formaldehyde was obtained by the Hantzsch method [65].

3. Results and discussions

Swollen hexagonal mesophases were used as soft templates to synthesize PPy nanostructures (PPy-NS-c). These mesophases consisted of oil-swollen surfactant tubes ordered on a triangular lattice in water [66,67]. The hydrophobic domain of the mesophases can be doped with high concentrations (up to 0.1 M) of PPy monomer, which is polymerized by the $FeCl_3$ oxidant. The mechanism of chemical oxidation of Py leading to PPy is described in the literature [68].

Other nanostructures of PPy were synthesized by radiolysis (PPy-NS-γ) [40]. Radiolysis of aqueous solution is an efficient way to polymerize monomers into polymers by oxidative hydroxyl radicals (Reaction (1)) [40]. Water radiolysis leads to formation of solvated electrons and radicals ($HO^{\cdot}$ and $H^{\cdot}$):

$$H_2O \xrightarrow{\gamma-\text{ radiation}} HO^{\bullet},\ e^-_{aq},\ H^{\bullet},\ H_2O_2,\ H_3O^+,\ H_2 \quad (1)$$

To scavenge electrons and produce more oxidative $HO^{\cdot}$ radicals, the aqueous solution is degassed with N_2O:

$$e^-_s + N_2O + H_2O \rightarrow HO^{\bullet} + HO^- + N_2 \quad (2)$$

Radiolytic polymerization of PPy is described in details [40].

3.1. Characterizations of PPy nanostrctures

SEM images present for PPy-NS-c homogeneous spherical nanostructures with an average size of 40 nm (Fig. 3a–b). Similar nanoparticles have been observed using TEM (Fig. S1). By contrast, PPy-NS-γ, synthesized by radiolysis, show nanoballs of uniform sizes of 400 nm (Fig. 3c–d), which correspond to the TEM images of PPy-NS-γ (Fig. S2). In case of chemical polymerization without template, amorphous particles connected in nacklaces are obtained (PPy-bulk) (Fig. 3e–f). Thanks to the confinement provided by the non-polar tubes of hexagonal mesophases used as soft template or γ-ray irradiation technique, we were able to control and direct the size and morphology of a variety of CPs, and hence to obtain polymer nanospheres.

The FTIR spectra of PPy-NS-c, PPy-NS-γ and PPy-bulk (Fig. 4) have been compared to those of PPy reported in the literature. [40,69–72] The major peaks in the 1400–1600 cm^{-1} region is related to the formation of the π conjugated polyene unit. The band located at 1420 cm^{-1} corresponds to the C–N stretching vibration from pyrrole ring, and the low intensity peak at 1550 cm^{-1} is ascribed to the C=C/C–C stretching of PPy, whereas peak at 1677 cm^{-1} could represent to C=N. The band of = C–H in plane-deformation vibration is situated at 1045 cm^{-1}.

Furthermore, no significant difference exists between the nanostructures synthesized by chemical oxidation or by radiolysis. Compared with PPy-bulk, some bands of PPy-NS-c and PPy-NS-γ are slightly shifted. The occurrence of small peak at 3284 cm^{-1} could be assigned to presence of N–H stretching vibrations. The main absorption bands of

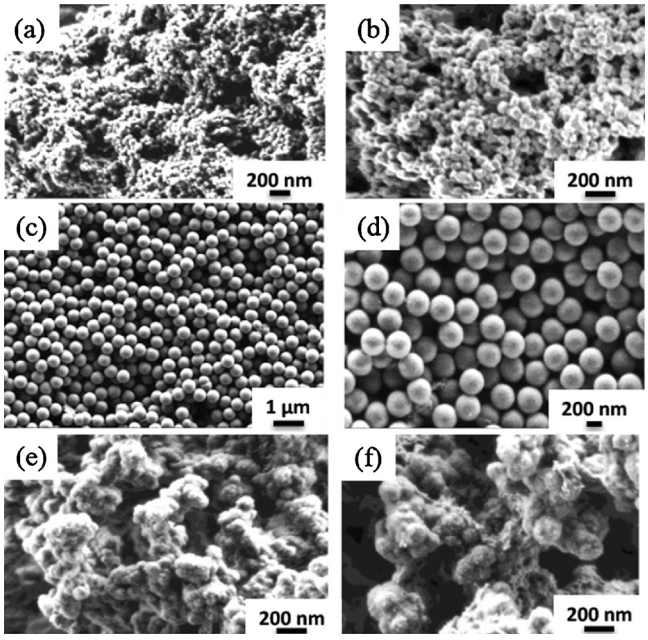

Fig. 3. SEM images of PPy-NS-c (a–b), PPy-NS-γ (c–d), and PPy-bulk (e–f).

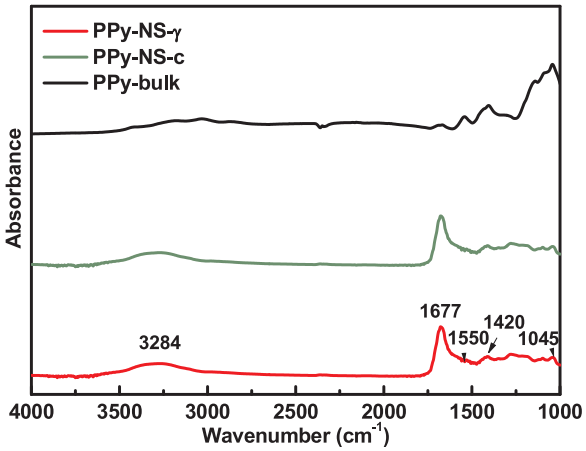

Fig. 4. ATR-FTIR spectra of PPy-NS-c, PPy-NS-γ, and PPy-bulk.

PPy-bulk are similar to PPy-NS-c and PPy-NS-γ and are shown in Fig. 4. These spectra revealed that PPy was successfully synthesized by chemical oxidative method and by radiolysis.

The maximum molecular weight of PPy-NS-c and PPy-NS-γ determined by Maldi-TOF mass spectroscopy was found to be respectively 1747 and 1709 g mol^{-1} corresponding to 26 and 25 repeated unite of Py monomers (See Figs. S3–4).

Fig. 5 shows UV–vis spectra recorded for a dispersion of PPy nanostructures in water. The spectra are similar to that in the previous reports [73–75]. The spectrum of PPy-NS-γ exhibits short wavelength absorption edge at about 425 nm, and the optical band gap is estimated equal to 2.41 eV. While PPy-NS-c shows absorption at shorter wavelength at 300 nm. Obviously, PPy-NS-c exhibits a small absorption in the visible region (≥ 400 nm), indicating that part of visible light can be transmitted through PPy solution. The peak at around 470 nm is due to the $\pi\text{-}\pi^*$ transitions [76]. Interestingly, there is a high absorption intensity from the visible region to near-IR region (700 nm ~ 1000 nm), which is the characteristic of the polaronic and bipolaronic transitions [56,75]. PPy-bulk agglomerates into larger particles that cannot be dispersed in ethanol and other solvents (The UV–vis spectrum of PPy-bulk powder is shown in Fig. S5).

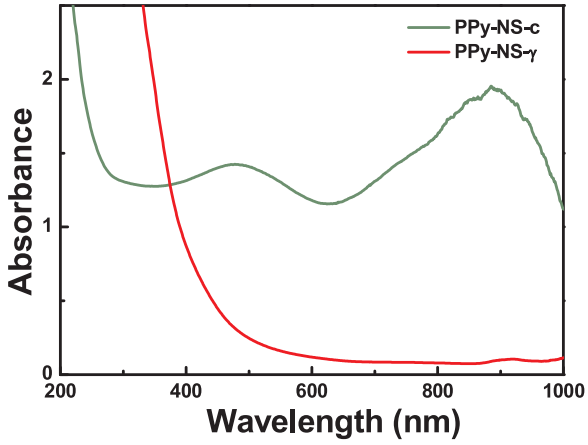

Fig. 5. UV–vis spectra of the PPy nanostructures (PPy-NS-c and PPy-NS-γ) and PPy-bulk in powder and in suspension.

To investigate the electrical conductivity of PPy, four-point probe technique was used to measure the resistance of the samples. The results show that PPy-NS-c nanostructures present the highest conductive performance. The electrical conductivity of the three samples, such as PPy-bulk, PPy-NS-γ and PPy-NS-c were 7.5×10^{-5} S cm^{-1}, 3.6×10^{-3} S cm^{-1}, 4.3×10^{-2} S cm^{-1}, respectively. It has to be noted that the conductivity increases drastically with the decreased diameter of the PPy particles and the smaller particles size corresponds to the higher surface area for electron transfer [77]. The highest conductivity of PPy-NS-c nanoparticles may be owing to smaller size, less defects, and larger surface areas. In fact, as the diameter decreases, the delocalization of charge carriers over an extended region of the polymer chains could be enhanced by higher surface area, and more ordered chains of connected structures of PPy-NS-c networks could counteract the influence of insulated cavities [40]. Similar results were obtained by our group for PDPB nanofibers synthesized in hexagonal mesophases. Indeed, the conductivity was found to increase with decreasing the diameter of the nanofibers [48].

3.2. Photocatalytic tests

The photocatalytic performance of the PPy samples was evaluated for degradation of phenol (initial concentration Co = 0.5 mM) and methyl orange (MO) (Co = 0.5 mM) in aqueous solution under UV and visible light irradiation. Phenol (taken as model pollutant) is stable under irradiation (no photolysis) and its intermediate degradation products are well known. Methyl orange, as an azo dye, is fairly stable (almost no photolysis was observed under solar light irradiation). Before irradiation, dark adsorption-desorption equilibrium and photolysis experiments were conducted. The rate of adsorption of phenol on PPy-NS-c is about 10% and the photolysis rate is about 3% after 5 h (Fig. S6). As shown in Fig. 6a, PPy-NS-c and PPy-NS-γ nanostructures exhibit higher degradation rate of phenol compared with PPy-bulk under UV light. Moreover, PPy-NS-c shows the best photocatalytic activity under UV light compared with PPy-NS-γ and PPy-bulk, with degradation rate of phenol about 100% after 4.5 h, while the photodegradation rate of PPy-NS-γ and PPy-bulk are about 80% and 37% after 5 h, respectively (Ag nanoparticles modified TiO_2 and P25 show the high activity under UV light). More interestingly, PPy-NS-γ showed a high photocatalytic activity under visible light. 20% degradation rate is achieved by PPy-NS-γ after 5 h irradiation whereas with PPy-NS-c and PPy-bulk, 10% and 5% degradation are reached respectively (Fig. 6b). This activity is close to that of plasmonic TiO_2 (TiO_2-P25 modified with Ag NPs) [78]. While the photocatalytic degradation of MO using PPy-NS-c is about 80% after 5 h under UV light and 10% under visible light, which is lower than phenol degradation (Fig. S7).

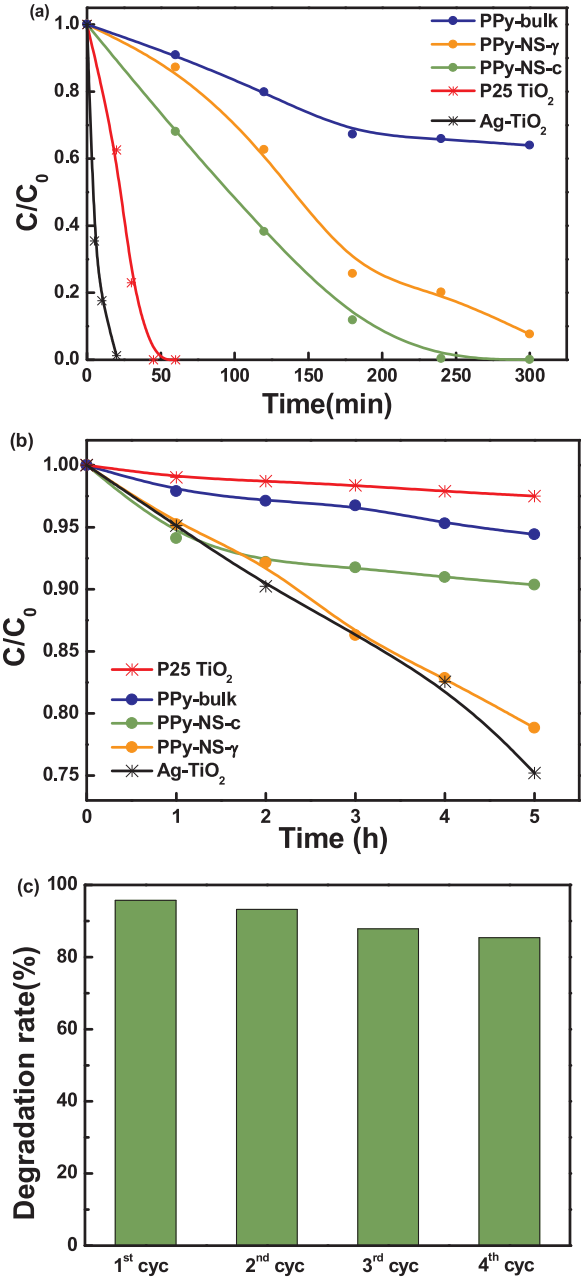

Fig. 6. Degradation rates of phenol in the presence of as-prepared samples of PPy under UV–vis (a) and visible light irradiation (b); (c) Photocatalytic activity of PPy-NS-c with cycling.

The total mineralization of phenol was followed using the value of the total organic carbon (TOC) for expressing the detoxification level of water. The PPy nanostructures are able to completely minerize the organic pollutants into CO_2 and H_2O. The results from TOC indicate that ~90% mineralization of phenol and ~79% mineralization of MO were achieved after 5 h irradiation (UV) with PPy-NS-c. Some related works on phenol degradation with different photocatalysts have been listed in Table S1 for comparison.

Furthermore, stability with cycling is another important factor for the applications in photocatalysis. In order to evaluate the stability of the conjugated polymer PPy nanostructures for practical application, the stability of PPy with cycling was studied. During the photocatalytic cycles, PPy NSs only shows a slight decrease trend, for example, the degradation rate of phenol is up to 87% at the fourth cycle (Fig. 6c) and there is no difference of morphology after 4 cycles (Fig. S8). This small

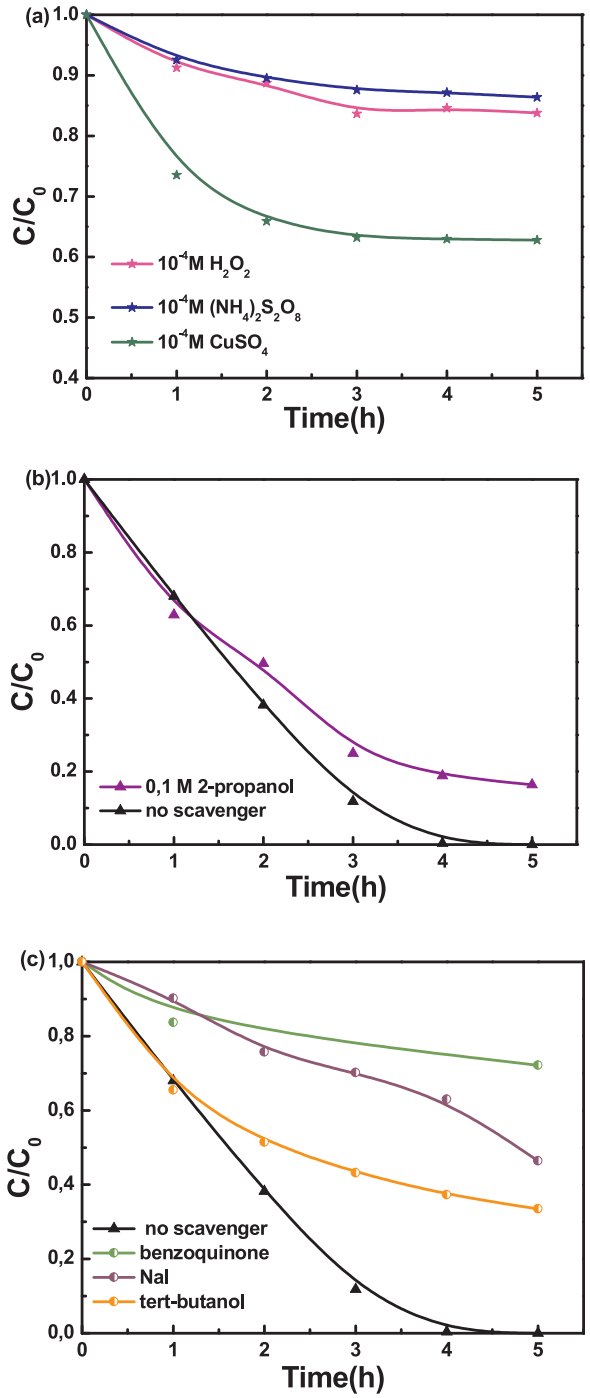

Fig. 7. Photocatalytic degradation of phenol using PPy-NS-c in the presence of (a) different electron scavengers, (b) both electron and hole scavengers, and **(c)** superoxide and hydroxyl radical scavengers.

decrease is due to the loss of the photocatalyst during the tests, as the samples are centrifuged and washed for further use. These results demonstrate that the as-prepared PPy NSs are very promising for water treatment and other photocatalytic applications. Our study also proves that nanostructuration of CPs is a key factor for photocatalytic applications. However, conjugated polymer nanostructures are very active photocatalysts under UV and visible light, while the bulk polymer counterparts have no significant photoactivity. The difference of photocatalytic activity between nanostructures and bulk CPs has been assigned to *(i)* the presence of more defects in bulk polymers favoring higher electron-hole recombination, and *(ii)* higher surface area with decreasing the size of the CPs [22,50].

3.3. Photocatalytic mechanism

We investigated the electronic properties of the synthesized PPy structures to understand their original photocatalytic activity under UV and visible light. When a semiconductor absorbs photons of energy higher or equal to its band gap, electrons (e^-) can be promoted from the valence band (VB) to the conduction band (CB), leaving holes (h^+) in the VB. Consequently, the e^- and h^+, when they escape recombination, can migrate to the surface of the photocatalysts where they participate in redox reactions with adsorbed species [79]. In the presence of dioxygen, e^- react with it to form the oxidizing superoxide radicals $O_2^{\cdot -}$ (E° ($O_2/O_2^{\cdot -}$) = −0.33 V_{SHE}) (Eq.1) and h^+ may be trapped by H_2O or HO^- to produce hydroxyl radicals ($HO^\cdot$) (Eqs. 2–4).

$$O_2 + e^- \rightarrow O_2^{\cdot -} \quad (1)$$

$O_2^{\cdot -}$ is a very reactive radical, so that it can oxidize molecules and $HO^\cdot$ can be formed through the following reactions:

$$O_2^{\cdot -} + H^+ \rightarrow HO_2^\cdot \quad (2)$$

$$2\ HO_2^\cdot \rightarrow H_2O_2 + O_2 \quad (3)$$

$$H_2O_2 + O_2^{\cdot -} \rightarrow HO^\cdot + O_2 + HO\text{-} \quad (4)$$

$$H_2O_2 + h^+ \rightarrow 2\ HO^\cdot \quad (5)$$

While in the HOMO level, the holes may react with HO^- (or H_2O) to produce oxidative HO)$^\cdot$ radicals:

$$H_2O + h^+ \rightarrow HO^\cdot + H^+ \quad (6)$$

These radicals are very active so that they can oxidize organic pollutants (such as phenol [80] and MO [81,82]) to form CO_2 and H_2O. Experiments were conducted in the presence of different scavengers to study the role of the radicals in the photocatalytic degradation process.

In the absence of O_2 (experiments under N_2 atmosphere) the activity of PPy-NS-c for phenol degradation decreases from 100% to 15% under UV and from 22% to 8% under visible light irradiation after 5 h, respectively (Figs. S9, S10). This indicates that the present of O_2 is an important factor during the photocatalytic process.

Fig. 7a shows phenol degradation in the presence of PPy-NS-c using different electron scavengers under UV light. The experiments were conducted in the presence of Cu^{2+} to scavenge electrons (forming Cu^+). The photodegradation rate of phenol is decreased from 100% to 87% in the presence of $CuSO_4$. Experiments with $CuSO_4$ show much lower degradation rates of phenol. Cu^{2+} reacts with electrons to produce Cu^+, which competes with reaction (1). The presence of Cu^{2+} leads to a decrease in $O_2^{\cdot -}$ concentration in the photocatalytic process, causing a decrease in the degradation kinetics.

Other electron scavengers (1×10^{-4} M of $(NH_4)_2O_8$ and 1×10^{-4} M of H_2O_2) were added to the suspension to investigate the photocatalytic activity. After 5 h, the photocatalytic degradation of phenol was 20% and 35% in the presence of $(NH_4)_2O_8$ and H_2O_2, respectively. These results indicate that addition of electron scavengers leads to lower photocatalytic degradation rate and Cu^{2+} are the most active species for scavenging electrons compared to the $(NH_4)_2O_8$ and H_2O_2.

2-propanol (0.1 M) was used as hole and $HO^\cdot$ scavenger. Fig. 7b shows that addition of 2-propanol does not affect the photodegradation rate (which is 85% after 5 h). Furthermore, to confirm the role of $HO^\cdot$ and $O_2^{\cdot -}$ radicals, tert-butanol and NaI were used as free $HO^\cdot$ and surface $HO^\cdot$ radical scavengers [79], and benzoquinone was used as the $O_2^{\cdot -}$ radical scavengers [23]. As shown in Fig. 7c, the rate of phenol degradation significantly decreases with benzoquinone ($O_2^{\cdot -}$ scavenger) addition indicating the crucial role of $O_2^{\cdot -}$ radical. In addition, it was found that the rate of photocatalytic degradation increased with NaI (surface $HO^\cdot$ radical scavenger) and tert-butanol (free $HO^\cdot$ radical

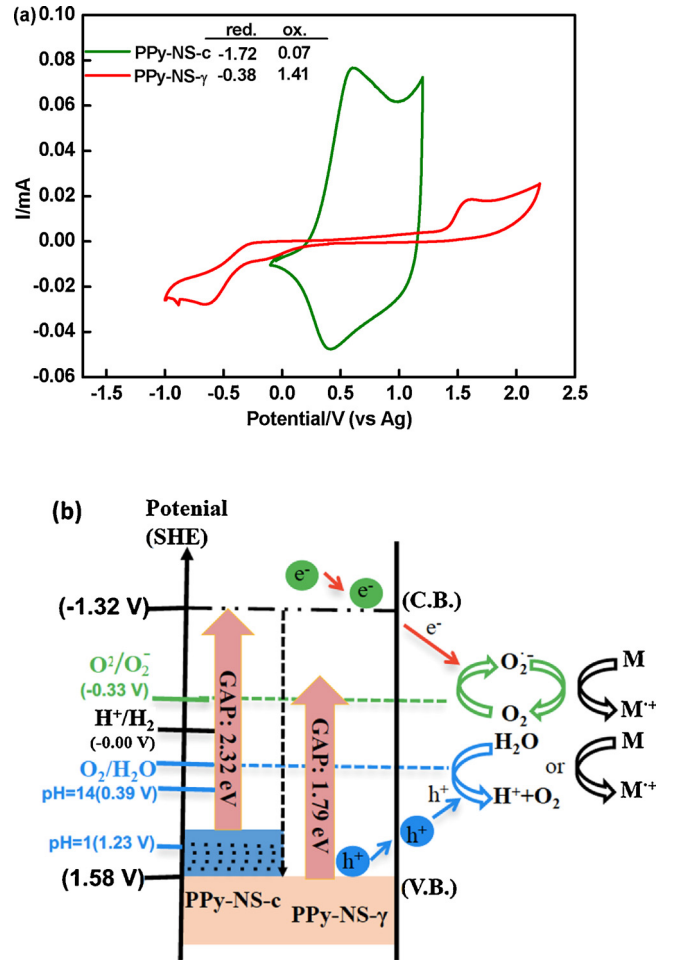

Fig. 8. (a) Cyclic Voltammetry of PPy recorded at 20 mV/s in acetonitrile and 0.1 M Tetrabutylammonium Perchlorate. Ferrocenium/ ferrocene (Fc/Fc^+) redox potential has been measured at the end of each experiment in order to calibrate the pseudo reference electrode (0.241 V *vs.* Ag in the present study). The energetic levels of PPy are obtained by the following equation: E_{HOMO} (eV) = − (4.8 + E_{ox_onset} − 0.241) and E_{LOMO} (eV) = − (4.8 + E_{red_onset} − 0.241). (b) Possible photocatalytic mechanism with charge separation in PPy nanostructures with electron reducing oxygen and the hole oxidizing water.

scavenger). The result also shows the surface HO˙ radicals are responsible for the degradation of phenol compared with free HO˙ radicals owing to the small detected quantity of HO˙ using Tris (hydroxymethy) aminomethane as a probe (Table S2) [64]. All these experiments demonstrate that photocatalytic degradation of phenol by PPy NS is mainly caused by $O_2^{\cdot -}$ superoxide radical (formed by the reaction of electron with dioxygen O_2).

To further understand the photocatalytic activity of PPy nanostructures, their electronic properties were investigated. Fig. 8a shows the cyclic voltammetry (CV) curve of PPy-NS-γ, PPy-NS-c and PPy-bulk, which was used to evaluate the energy levels of the lowest unoccupied molecular orbital (LUMO) and the highest occupied molecular orbital (HOMO) from the ionization potential and the electronic affinity, and the band gap of PPy is calculated (Fig. S11, Table S3). Specifically, the primaryoxidation (p-doping) process occurs at onset potentials of 0.07 V (PPy-NS-c) and 1.41 V (PPy-NS- γ), while reduction (n-doping) process starts at −1.72 V (PPy-NS-c) and -0.38 V (PPy-NS- γ). The energy levels of the LUMO/HOMO, for PPy-NS-γ and PPy-NS-c were respectively determined: −4.18 eV/−5.97 eV and −2.84 eV/−5.16 eV. The band gap was estimated to be 1.79 eV and 2.32 eV, respectively, which are remarkably smaller than the band gap of TiO_2 (3.20 eV). Actually, lower band gap implies the possibility of activation of the polymer nanostructures under visible light with potential application in optoelectronics, photocatalysis or eletrocatalysis. Recently, in our group, CP nanostructures of PDPB, P3HT and PEDOT with small band gaps and high photocatalytic activity under visible light were developed [23,51,52].

Based on the above results, a possible photocatalytic mechanism of PPy nanostructures was proposed as illustrated in Fig. 8**b**. The generated charge carriers under both UV or visible light irradiation and the reactive oxygen species (ROS) are responsible for the oxidation and the organic pollutant (phenol or MO) degradation. Our results indicate that $O_2^{\cdot -}$ is the main radical responsible of degradation of the organic pollutant and their mineralization.

The optical band gap energy (E_g) of PPy was estimated by Kubelka-Munk method. The corresponding E_g can be determined by the linear portion of $(\alpha h\nu)^n$ *vs.* $(h\nu)$ plot, where α, h, ν and k are the absorption coefficient, Planck constant, and light frequency, respectively. The value of n is equal to 2 for the indirect bandgap and 1/2 for the direct bandgap. Fig. 9 presents the Kubelka-Munk plots for PPy samples used to estimate the E_g associated with the direct transitions. As a result, the E_g of PPy-NS- γ and PPy-NS-c is about 1.94 eV and 2.01 eV. The results are quite similar to the band gap of PPy-NSs from CV calculation (Fig. 8 and Table S2). The variation of the band gap values obtained by calculation by Kubelka-Munk and CV methods can be explained by numerous reasons, which include geometrical arrangement and electronic configuration of the constituting elements, charge imbalance, oxygen vacancies and defects on the polymer surface.

4. Conclusions

PPy nanostructures were obtained by two different methods of

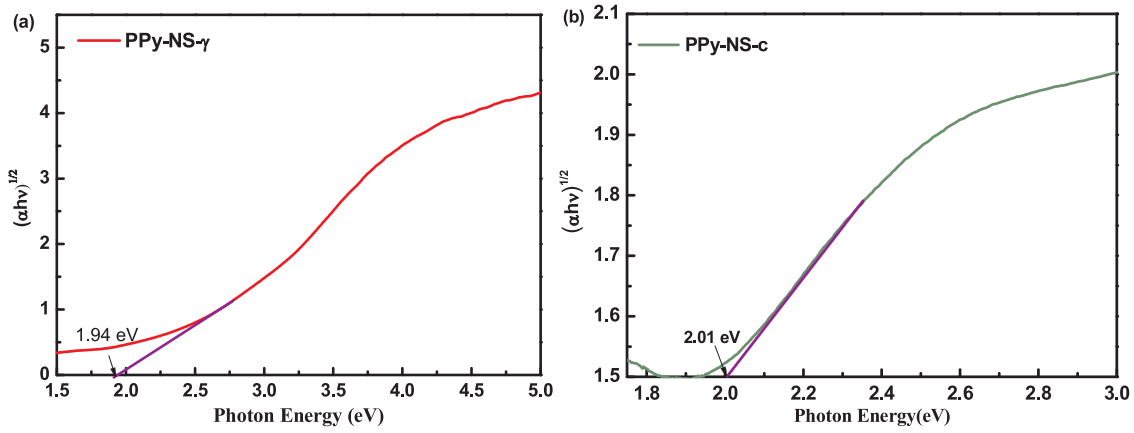

Fig. 9. Kubelka-Munk plots and band gap energy estimation of PPy-NS-γ (a) and PPy-NS-c (b) for direct transition.

polymerization: PPy-NS-c were successfully synthesized by chemical oxidation with Fe^{3+} in hexagonal mesophases (used as soft templates) and PPy-NS-γ were obtained by radiolytic polymerization. PPy-NS-c and PPy-NS-γ nanostructures show much higher photocatalytic activities under ultraviolet and visible light irradiation compared with PPy-bulk (synthesized without any template). The photocatalytic activity of the PPy nanostructures is close to that of plasmonic silver nanoparticles modified TiO_2 under visible light. Our experiments demonstrate that $O_2^{\cdot -}$ radicals are the main radical responsible for the degradation of phenol and MO. Nanostructuration of the CP is a key factor for their application in photocatalysis. These photocatalysts are stable with cycling. These results open interesting perspectives of using conjugated polymer nanostructures for different applications in photocatalysis: water and air treatment, self-cleaning surfaces and water splitting. Further studies will focus on design of composite materials based PPy heterojunctions for efficient solar hydrogen conversion and solar fuel production.

Acknowledgements

X.Y. gratefully acknowledges the financial support from China Scholarship Council (CSC). The authors thank Patricia Beaunier (LRS, UPMC, Sorbonne Université) for TEM observations. The authors acknowledge the IDEX Paris-Saclay and IRS MOMENTOM for financial support.

Appendix A. Supplementary data

Supplementary material related to this article can be found, in the online version, at doi:https://doi.org/10.1016/j.apcatb.2018.10.002.

References

[1] G. Wang, L. Xu, J. Zhang, T. Yin, D. Han, Enhanced photocatalytic activity of powders (P25) via calcination treatment, Int. J. Photoenergy 2012 (2012) 1–9.
[2] M. Méndez-Medrano, E. Kowalska, A. Lehoux, A. Herissan, B. Ohtani, S. Rau, C. Colbeau-Justin, J. Rodríguez-López, H. Remita, Surface modification of TiO_2 with Au nanoclusters for efficient water treatment and hydrogen generation under visible light, J. Phys. Chem. C 120 (2016) 25010–25022.
[3] D. Yang, Y. Sun, Z. Tong, Y. Tian, Y. Li, Z. Jiang, Synthesis of Ag/TiO_2 nanotube heterojunction with improved visible-light photocatalytic performance inspired by bioadhesion, J. Phys. Chem. C 119 (2015) 5827–5835.
[4] L. Wu, F. Li, Y. Xu, J.W. Zhang, D. Zhang, G. Li, H. Li, Plasmon-induced photoelectrocatalytic activity of Au nanoparticles enhanced TiO_2 nanotube arrays electrodes for environmental remediation, Appl. Catal. B: Environ. 164 (2015) 217–224.
[5] B. Sambandam, A. Surenjan, L. Philip, T. Pradeep, Rapid synthesis of C-TiO_2: tuning the shape from spherical to rice grain morphology for visible light photocatalytic application, ACS Sustain. Chem. Eng. 3 (2015) 1321–1329.
[6] G. Mishra, K. Parida, S. Singh, Facile fabrication of S-TiO_2/β-SiC nanocomposite photocatalyst for hydrogen evolution under visible light irradiation, ACS Sustain. Chem. Eng. 3 (2015) 245–253.
[7] G.N. Nomikos, P. Panagiotopoulou, D.I. Kondarides, X.E. Verykios, Kinetic and mechanistic study of the photocatalytic reforming of methanol over Pt/TiO_2 catalyst, Appl. Catal. B: Environ. 146 (2014) 249–257.
[8] X.-j. Wang, W.-y. Yang, F.-t. Li, Y.-b. Xue, R.-h. Liu, Y.-j. Hao, In situ microwave-assisted synthesis of porous N-TiO_2/g-C_3N_4 heterojunctions with enhanced visible-light photocatalytic properties, Ind. Eng. Chem. Res. 52 (2013) 17140–17150.
[9] M.N. Chong, B. Jin, C.W. Chow, C. Saint, Recent developments in photocatalytic water treatment technology: a review, Water Res. 44 (2010) 2997–3027.
[10] A. Rostami-Vartooni, M. Nasrollahzadeh, M. Salavati-Niasari, M. Atarod, Photocatalytic degradation of azo dyes by titanium dioxide supported silver nanoparticles prepared by a green method using Carpobrotus acinaciformis extract, J. Alloys Compd. 689 (2016) 15–20.
[11] H. Cheng, B. Huang, Y. Dai, Engineering BiOX (X= Cl, Br, I) nanostructures for highly efficient photocatalytic applications, Nanoscale 6 (2014) 2009–2026.
[12] C. Zhou, C. Lai, P. Xu, G. Zeng, D. Huang, C. Zhang, M. Cheng, L. Hu, J. Wan, Y. Liu, In situ grown AgI/$Bi_{12}O_{17}Cl_2$ heterojunction photocatalysts for visible light degradation of sulfamethazine: efficiency, pathway, and mechanism, ACS Sustain. Chem. Eng. 6 (2018) 4174–4184.
[13] S. Zinatloo-Ajabshir, M.S. Morassaei, M. Salavati-Niasari, $Nd_2Sn_2O_7$ nanostructures as highly efficient visible light photocatalyst: Green synthesis using pomegranate juice and characterization, J. Clean. Prod. 198 (2018) 11–18.
[14] S. Zinatloo-Ajabshir, M.S. Morassaei, M. Salavati-Niasari, Facile fabrication of $Dy_2Sn_2O_7$-SnO_2 nanocomposites as an effective photocatalyst for degradation and removal of organic contaminants, J. Colloid Interface Sci. 497 (2017) 298–308.
[15] M.S. Morassaei, S. Zinatloo-Ajabshir, M. Salavati-Niasari, $Nd_2Sn_2O_7$ nanostructures: new facile Pechini preparation, characterization, and investigation of their photocatalytic degradation of methyl orange dye, Adv. Powder Technol. 28 (2017) 697–705.
[16] M.S. Morassaei, S. Zinatloo-Ajabshir, M. Salavati-Niasari, New facile synthesis, structural and photocatalytic studies of NdOCl-$Nd_2Sn_2O_7$-SnO_2 nanocomposites, J. Mol. Liq. 220 (2016) 902–909.
[17] A. Abbasi, M. Hamadanian, M. Salavati-Niasari, S. Mortazavi-Derazkola, Facile size-controlled preparation of highly photocatalytically active $ZnCr_2O_4$ and $ZnCr_2O_4$/Ag nanostructures for removal of organic contaminants, J. Colloid Interface Sci. 500 (2017) 276–284.
[18] M. Hassanpour, H. Safardoust-Hojaghan, M. Salavati-Niasari, Degradation of methylene blue and Rhodamine B as water pollutants via green synthesized Co_3O_4/ZnO nanocomposite, J. Mol. Liq. 229 (2017) 293–299.
[19] G. Liao, S. Chen, X. Quan, H. Yu, H. Zhao, Graphene oxide modified g-C_3N_4 hybrid with enhanced photocatalytic capability under visible light irradiation, J. Mater. Chem. 22 (2012) 2721–2726.
[20] H. Safardoust-Hojaghan, M. Salavati-Niasari, Degradation of methylene blue as a pollutant with N-doped graphene quantum dot/titanium dioxide nanocomposite, J. Clean. Prod. 148 (2017) 31–36.
[21] M. Mahdiani, A. Sobhani, M. Salavati-Niasari, Enhancement of magnetic, electrochemical and photocatalytic properties of lead hexaferrites with coating graphene and CNT: sol-gel auto-combustion synthesis by valine, Sep. Purif. Technol. 185 (2017) 140–148.
[22] S. Ghosh, N.A. Kouamé, L. Ramos, S. Remita, A. Dazzi, A. Deniset-Besseau, P. Beaunier, F. Goubard, P.-H. Aubert, H. Remita, Conducting polymer nanostructures for photocatalysis under visible light, Nat. Mater. 14 (2015) 505–511.
[23] D. Floresyona, F. Goubard, P.-H. Aubert, I. Lampre, J. Mathurin, A. Dazzi, S. Ghosh, P. Beaunier, F. Brisset, S. Remita, L. Ramos, H. Remita, Highly active poly (3-hexylthiophene) nanostructures for photocatalysis under solar light, Appl. Catal. B: Environ. 209 (2017) 23–32.
[24] D.B. Kayan, F. Köleli, Simultaneous electrocatalytic reduction of dinitrogen and carbon dioxide on conducting polymer electrodes, Appl. Catal. B: Environ. 181 (2016) 88–93.
[25] K. Wang, H. Wu, Y. Meng, Z. Wei, Conducting polymer nanowire arrays for high performance supercapacitors, Small 10 (2014) 14–31.
[26] Z. Yin, Q. Zheng, Controlled synthesis and energy applications of one-dimensional conducting polymer nanostructures: an overview, Adv. Energy Mater. 2 (2012) 179–218.
[27] S.-Y. Huang, P. Ganesan, B.N. Popov, Development of conducting polypyrrole as corrosion-resistant catalyst support for polymer electrolyte membrane fuel cell (PEMFC) application, Appl. Catal. B: Environ. 93 (2009) 75–81.
[28] C. Chiang, Y.-W. Park, A. Heeger, H. Shirakawa, E. Louis, A.G. MacDiarmid, Conducting polymers: halogen doped polyacetylene, J. Chem. Phys. 69 (1978) 5098–5104.
[29] C.K. Chiang, C. Fincher Jr, Y.W. Park, A.J. Heeger, H. Shirakawa, E.J. Louis, S.C. Gau, A.G. MacDiarmid, Electrical conductivity in doped polyacetylene, Phys. Rev. Lett. 39 (1977) 1098.
[30] S. Ghosh, A.-L. Teillout, D. Floresyona, P. de Oliveira, A. Hagège, H. Remita, Conducting polymer-supported palladium nanoplates for applications in direct alcohol oxidation, Int. J. Hydrogen Energy 40 (2015) 4951–4959.
[31] S. Ghosh, S. Bera, S. Bysakh, R.N. Basu, Highly active multimetallic palladium nanoalloys embedded in conducting polymer as anode catalyst for electrooxidation of ethanol, ACS Appl. Mater. Interfaces 9 (2017) 33775–33790.
[32] S. Ghosh, T. Maiyalagan, R.N. Basu, Nanostructured conducting polymers for energy applications: towards a sustainable platform, Nanoscale 8 (2016) 6921–6947.
[33] S. Sardar, P. Kar, H. Remita, B. Liu, P. Lemmens, S.K. Pal, S. Ghosh, Enhanced charge separation and FRET at heterojunctions between semiconductor nanoparticles and conducting polymer nanofibers for efficient solar light harvesting, Sci. Rep. 5 (2015) 17313.
[34] S. Ghosh, R.N. Basu, H. Remita, Conducting polymers nanostructures as novel materials for efficient solar light harvesting, in: S. Ghosh (Ed.), Visible-Light-Active Photocatalysis: Nanostructured Catalyst Design, Mechanisms, and Applications, Wiley-VCH Verlag Gmbh & Co. KGaA, 2018, pp. 227–252. April, Chapter 9.
[35] X. Wang, K. Maeda, A. Thomas, K. Takanabe, G. Xin, J.M. Carlsson, K. Domen, M. Antonietti, A metal-free polymeric photocatalyst for hydrogen production from water under visible light, Nat. Mater. 8 (2009) 76.
[36] Y. Wang, H. Li, J. Yao, X. Wang, M. Antonietti, Synthesis of boron doped polymeric carbon nitride solids and their use as metal-free catalysts for aliphatic C–H bond oxidation, Chem. Sci. 2 (2011) 446–450.
[37] C. Zhou, C. Lai, D. Huang, G. Zeng, C. Zhang, M. Cheng, L. Hu, J. Wan, W. Xiong, M. Wen, Highly porous carbon nitride by supramolecular preassembly of monomers for photocatalytic removal of sulfamethazine under visible light driven, Appl. Catal. B: Environ. 220 (2018) 202–210.
[38] C. Zhou, C. Lai, P. Xu, G. Zeng, D. Huang, Z. Li, C. Zhang, M. Cheng, L. Hu, J. Wan, Rational design of carbon-doped carbon Nitride/$Bi_{12}O_{17}Cl_2$ composites: a promising candidate photocatalyst for boosting visible-light-driven photocatalytic degradation of tetracycline, ACS Sustain. Chem. Eng. 6 (2018) 6941–6949.
[39] C. Zhou, C. Lai, C. Zhang, G. Zeng, D. Huang, M. Cheng, L. Hu, W. Xiong, M. Chen, J. Wang, Semiconductor/boron nitride composites: synthesis, properties, and photocatalysis applications, Appl. Catal. B: Environ. 238 (2018) 6–18.
[40] Z. Cui, C. Coletta, A. Dazzi, P. Lefrancois, M. Gervais, S. Néron, S. Remita, Radiolytic method as a novel approach for the synthesis of nanostructured conducting polypyrrole, Langmuir 30 (2014) 14086–14094.
[41] T. Bahry, Z. Cui, A. Deniset, M. Gervais, B. Thanh-Tuân, S. REMITA, An alternative

radiolytic route for synthesizing conducting polymers in an organic solvent, New J. Chem. 42 (2018) 8704–8716.
[42] Y. Lattach, A. Deniset-Besseau, J.-M. Guigner, S. Remita, Radiation chemistry as an alternative way for the synthesis of PEDOT conducting polymers under “soft” conditions, Radiat. Phys. Chem. 82 (2013) 44–53.
[43] Y. Lattach, C. Coletta, S. Ghosh, S. Remita, Radiation-induced synthesis of nanostructured conjugated polymers in aqueous solution: fundamental effect of oxidizing species, ChemPhysChem 15 (2014) 208–218.
[44] C. Coletta, Z. Cui, P. Archirel, P. Pernot, J.-L. Marignier, S. Remita, Electron-induced growth mechanism of conducting polymers: a coupled experimental and computational investigation, J. Phys. Chem. B 119 (2015) 5282–5298.
[45] Z. Cui, C. Coletta, R. Rebois, S. Baiz, M. Gervais, F. Goubard, P.-H. Aubert, A. Dazzi, S. Remita, Radiation-induced reduction–polymerization route for the synthesis of PEDOT conducting polymers, Radiat. Phys. Chem. 119 (2016) 157–166.
[46] C. Coletta, Z. Cui, A. Dazzi, J.-M. Guigner, S. Néron, J.-L. Marignier, S. Remita, A pulsed electron beam synthesis of PEDOT conducting polymers by using sulfate radicals as oxidizing species, Radiat. Phys. Chem. 126 (2016) 21–31.
[47] Z. Cui, C. Coletta, T. Bahry, J.-L. Marignier, J.-M. Guigner, M. Gervais, S. Baiz, F. Goubard, S. Remita, A novel radiation chemistry-based methodology for the synthesis of PEDOT/Ag nanocomposites, Mater. Chem. Front. 1 (2017) 879–892.
[48] S. Ghosh, L. Ramos, S. Remita, A. Dazzi, A. Deniset-Besseau, P. Beaunier, F. Goubard, P.-H. Aubert, H. Remita, Conducting polymer nanofibers with controlled diameters synthesized in hexagonal mesophases, New J. Chem. 39 (2015) 8311–8320.
[49] S. Ghosh, N.A. Kouame, S. Remita, L. Ramos, F. Goubard, P.-H. Aubert, A. Dazzi, A. Deniset-Besseau, H. Remita, Visible-light active conducting polymer nanostructures with superior photocatalytic activity, Sci. Rep. 5 (2015) 18002.
[50] S. Ghosh, L. Ramos, H. Remita, Swollen hexagonal liquid crystals as smart nanoreactors: implementation in materials chemistry for energy applications, Nanoscale 10 (2018) 5793–5819.
[51] S. Ghosh, H. Remita, L. Ramos, A. Dazzi, A. Deniset-Besseau, P. Beaunier, F. Goubard, P.-H. Aubert, F. Brisset, S. Remita, PEDOT nanostructures synthesized in hexagonal mesophases, New J. Chem. 38 (2014) 1106–1115.
[52] S. Ghosh, N.A. Kouamé, L. Ramos, S. Remita, A. Dazzi, A. Deniset-Besseau, P. Beaunier, F. Goubard, P.-H. Aubert, H. Remita, Conducting polymer nanostructures for photocatalysis under visible light, Nat. Mater. 14 (2015) 505–511.
[53] S. Naficy, N. Stoboi, P.G. Whitten, G.M. Spinks, G.G. Wallace, Evaluation of encapsulating coatings on the performance of polypyrrole actuators, Smart Mater. Struct. 22 (2013) 075005.
[54] Y. Shi, L. Pan, B. Liu, Y. Wang, Y. Cui, Z. Bao, G. Yu, Nanostructured conductive polypyrrole hydrogels as high-performance, flexible supercapacitor electrodes, J. Mater. Chem. A 2 (2014) 6086–6091.
[55] Y. Huang, J. Tao, W. Meng, M. Zhu, Y. Huang, Y. Fu, Y. Gao, C. Zhi, Super-high rate stretchable polypyrrole-based supercapacitors with excellent cycling stability, Nano Energy 11 (2015) 518–525.
[56] Z. Zha, X. Yue, Q. Ren, Z. Dai, Uniform polypyrrole nanoparticles with high photothermal conversion efficiency for photothermal ablation of cancer cells, Adv. Mater. 25 (2013) 777–782.
[57] S. Jeon, J.M. Moon, E.S. Lee, Y.H. Kim, Y. Cho, An electroactive biotin-doped polypyrrole substrate that immobilizes and releases EpCAM-positive cancer cells, Angew. Chem. 126 (2014) 4685–4690.
[58] T. Yao, T. Cui, H. Wang, L. Xu, F. Cui, J. Wu, A simple way to prepare Au@polypyrrole/Fe_3O_4 hollow capsules with high stability and their application in catalytic reduction of methylene blue dye, Nanoscale 6 (2014) 7666–7674.
[59] S. De Vito, C.R. Martin, Toward colloidal dispersions of template-synthesized polypyrrole nanotubules, Chem. Mater. 10 (1998) 1738–1741.
[60] Y. Yang, M. Wan, Microtubules of polypyrrole synthesized by an electrochemical template-free method, J. Mater. Chem. 11 (2001) 2022–2027.
[61] D. Wang, Y. Wang, X. Li, Q. Luo, J. An, J. Yue, Sunlight photocatalytic activity of polypyrrole–TiO_2 nanocomposites prepared by ‘in situ’method, Catal. Commun. 9 (2008) 1162–1166.
[62] S. Gu, B. Li, C. Zhao, Y. Xu, X. Qian, G. Chen, Preparation and characterization of visible light-driven AgCl/PPy photocatalyst, J. Alloys Compd. 509 (2011) 5677–5682.
[63] Q. Wang, L. Zheng, Y. Chen, J. Fan, H. Huang, B. Su, Synthesis and characterization of novel PPy/$Bi_2O_2CO_3$ composite with improved photocatalytic activity for degradation of Rhodamine-B, J. Alloys Compd. 637 (2015) 127–132.
[64] V. Diesen, M. Jonsson, Tris (hydroxymethyl) aminomethane as a probe in heterogeneous TiO_2 photocatalysis, J. Adv. Oxid. Technol. 15 (2012) 392–398.
[65] L. Qiong, P. Sritharathikhun, S. Motomizu, Development of novel reagent for Hantzsch reaction for the determination of formaldehyde by spectrophotometry and fluorometry, Anal. Sci. 23 (2007) 413–417.
[66] E. Pena dos Santos, M.S. Tokumoto, G. Surendran, H. Remita, C. Bourgaux, P. Dieudonné, E. Prouzet, L. Ramos, Existence and stability of new nanoreactors: highly swollen hexagonal liquid crystals, Langmuir 21 (2005) 4362–4369.
[67] G. Surendran, M.S. Tokumoto, E. Pena dos Santos, H. Remita, L. Ramos, P.J. Kooyman, C.V. Santilli, C. Bourgaux, P. Dieudonné, E. Prouzet, Highly swollen liquid crystals as new reactors for the synthesis of nanomaterials, Chem. Mater. 17 (2005) 1505–1514.
[68] M. Wang, Emerging multifunctional NIR photothermal therapy systems based on polypyrrole nanoparticles, Polymers 8 (2016) 373.
[69] Y. Wang, Z. Lu, Z. Zhu, X. Zhao, N. Gao, D. Wang, Z. Hua, Y. Yan, P. Huo, M. Song, Enhanced selective photocatalytic properties of a novel magnetic retrievable imprinted $ZnFe_2O_4$/PPy composite with specific recognition ability, RSC Adv. 6 (2016) 51877–51887.
[70] C. MA, P. SG, S. Shashwati, Synthesis and characterization of polypyrrole (PPy) thin films, Soft Nanosci. Lett. 1 (2011) 6–10.
[71] M. Karim, C. Lee, M. Lee, Synthesis of conducting polypyrrole by radiolysis polymerization method, Polym. Adv. Technol. 18 (2007) 916–920.
[72] S. Ghosh, N. Bhandary, S. Basu, R.N. Basu, Synergistic effects of polypyrrole nanofibers and Pd nanoparticles for improved electrocatalytic performance of Pd/PPy nanocomposites for ethanol oxidation, Electrocatalysis 8 (2017) 329–339.
[73] J. Nayak, S.K. Mahadeva, J. Kim, Characteristics of flexible electrode made on cellulose by soluble polypyrrole coating, Proc. Inst. Mech. Eng. Part C: J. Mech. Eng. Sci. 226 (2012) 2605–2609.
[74] M.A. Chougule, S.G. Pawar, P.R. Godse, R.N. Mulik, S. Sen, V.B. Patil, Synthesis and characterization of polypyrrole (PPy) thin films, Soft Nanosci. Lett. 1 (2011) 6.
[75] X. Chen, N. Yu, L. Zhang, Z. Liu, Z. Wang, Z. Chen, Synthesis of polypyrrole nanoparticles for constructing full-polymer UV/NIR-shielding film, RSC Adv. 5 (2015) 96888–96895.
[76] K.-J. Ahn, Y. Lee, H. Choi, M.-S. Kim, K. Im, S. Noh, H. Yoon, Surfactant-templated synthesis of polypyrrole nanocages as redox mediators for efficient energy storage, Sci. Rep. 5 (2015) 14097.
[77] N. Paradee, A. Sirivat, Synthesis of poly (3, 4-ethylenedioxythiophene) nanoparticles via chemical oxidation polymerization, Polym. Int. 63 (2014) 106–113.
[78] A.L. Luna, D. Dragoe, K. Wang, P. Beaunier, E. Kowalska, B. Ohtani, D. Bahena Uribe, M.A. Valenzuela, H. Remita, C. Colbeau-Justin, Photocatalytic hydrogen evolution using Ni–Pd/TiO_2: correlation of light absorption, charge-carrier dynamics, and quantum efficiency, J. Phys. Chem. C 121 (2017) 14302–14311.
[79] B. Abramović, V. Despotović, D. Šojić, N. Finčur, Mechanism of clomazone photocatalytic degradation: hydroxyl radical, electron and hole scavengers, React. Kinet. Mech. Catal. 115 (2015) 67–79.
[80] Y. Tao, Z. Cheng, K. Ting, X. Yin, Photocatalytic degradation of phenol using a nanocatalyst: the mechanism and kinetics, J. Catal. 2013 (2012) 1–6.
[81] T. Chen, Y. Zheng, J.-M. Lin, G. Chen, Study on the photocatalytic degradation of methyl orange in water using Ag/ZnO as catalyst by liquid chromatography electrospray ionization ion-trap mass spectrometry, J. Am. Soc. Mass Spectrom. 19 (2008) 997–1003.
[82] M.S. Morassaei, S. Zinatloo-Ajabshir, M. Salavati-Niasari, Simple salt-assisted combustion synthesis of $Nd_2Sn_2O_7$–SnO_2 nanocomposites with different amino acids as fuel: an efficient photocatalyst for the degradation of methyl orange dye, J. Mater. Sci. Mater. Electron. 27 (2016) 11698–11706.